ADVANCED ENERGY & SUSTAINABILITY RESEARCH
www.advenergysustres.com

# Catalytic Activity of Solution Additive Anions for Magnesite and Calcite Precipitation in Microwave-Assisted Mineral Carbonation Experiments

*Marcello Campione,* Daniela D'Alessio, Mattia Corti, Giancarlo Capitani, Andrea Lucotti, Matteo Tommasini, Rossella Yivlialin, Lamberto Duò, Gianlorenzo Bussetti, and Nadia Malaspina*

**Identifying catalytic routes for magnesite and calcite precipitation from Mg- and Ca-bearing minerals is key to developing carbon-neutral or negative industrial processes. This study experimentally evaluates the catalytic activity of over 20 environmentally friendly additive anions—including carboxylates, inorganics, and ammonium salts—for promoting magnesite and calcite formation during the carbonation of brucite [$Mg(OH)_2$] and portlandite [$Ca(OH)_2$] in aqueous slurries. Carbonation is driven by microwave (MW)-assisted heating at 100–200 °C under hydrothermal conditions, with $CO_2$ partial pressures below 8 bar. Results reveal a significant enhancement in magnesite precipitation when additives are combined with MW energy, enabling crystallization at much lower temperatures. For calcite, MWs alone nearly double the precipitation yield, with further improvements in the presence of additives. Among promising catalyzers, chelating agents like citrate and tartrate increase induction times and reduce overall yield at higher concentrations. In contrast, additives forming simple ion pairs—such as acetate and sulfate—show improved performance with increased concentration. These findings highlight the importance of additive selection and MW energy in optimizing mineral carbonation for sustainable applications.**

## 1. Introduction

Magnesium and calcium are among the most abundant rock-forming metals within the Earth's lithosphere and are particularly concentrated in the oceanic crust. Thanks to their ability to naturally form insoluble hydroxy-carbonate hydrates and carbonates, these elements are key for the future development of carbon capture, utilization and storage (CCUS) methodologies.[1,2] Indeed, mineral carbonation (MC) is a natural process that usually occurs in mine tailings and/or waste when Mg- or Ca-rich silicates (e.g., olivine, serpentine, clinopyroxene) or hydroxides (e.g., brucite, portlandite) react in water environment with carbon dioxide (preferably contained in a flue gas) to form stable compounds storing carbon, usually in the form of carbonates, and possibly enabling their use as secondary raw materials. In principle, several Mg- and Ca-bearing minerals, such as oxides, hydroxides, and silicates with various hydration levels, can be used as reactants in carbonation reactions with the scope of producing insoluble carbonates. However, though spontaneous, this reaction is affected by kinetic barriers that hinder its effective exploitation in industrial applications. One of the most challenging aspects of this reaction is the possibility of precipitating anhydrous magnesite ($MgCO_3$) at low temperature. Indeed, even though $MgCO_3$ is the thermodynamically most stable Mg-carbonate polymorph,[3] magnesium hydroxy-carbonate hydrates (MHCHs) are kinetically favored at temperatures lower than 200 °C.[4] MHCHs find useful application as additives in construction compounds;[5] however, their lower economic value, lower stability, and their tendency to capture also a fraction of environmental water make them far less attractive than

M. Campione, D. D'Alessio, M. Corti, G. Capitani, N. Malaspina
Department of Earth and Environmental Sciences
University of Milano – Bicocca
Piazza della Scienza 4, I-20126 Milano, Italy
E-mail: marcello.campione@unimib.it

The ORCID identification number(s) for the author(s) of this article can be found under https://doi.org/10.1002/aesr.202500046.



**DOI: 10.1002/aesr.202500046**

A. Lucotti, M. Tommasini
Department of Chemistry
Materials and Chemical Engineering
Politecnico di Milano
Piazza Leonardo da Vinci 32, I-20133 Milano, Italy

R. Yivlialin, L. Duò, G. Bussetti
Department of Physics
Politecnico di Milano
Piazza Leonardo da Vinci 32, I-20133 Milano, Italy

magnesite. On the contrary, aqueous precipitation of the thermodynamically most stable Ca-carbonate, i.e., calcite, $CaCO_3$, is not kinetically hindered at room temperature,[6,7] making this step of MC less critical, even though deserving in-depth investigations to achieve optimization and address the more complex problem of promoting the precipitation of Mg- and Ca-carbonates from mixtures containing both metal ions.[8]

Different attempts have been undertaken to induce the direct precipitation of magnesite at low temperatures. Partial pressures of $CO_2$ as high as 90–110 atm were observed to facilitate the progressive transformation of MHCH into magnesite at temperatures lower than 50 °C. However, reaction times were of the order of tens of days.[9] Within time lapses of the same order, direct magnesite precipitation at room temperature was observed on the surface of carboxylated polystyrene microspheres.[10] Using citrate tri-potassic salt 2 M added to a brucite slurry under continuous $CO_2$ bubbling in a pressure vessel maintained at 150 °C and 7 bar, magnesite was obtained in a time reduced by 50%, from 12 to 6 h.[11] By using massive amounts of NaOH as $CO_2$ sequestering agent, magnesite was obtained at 90 °C with 50 bar of $CO_2$ pressure after 15 h of treatment.[12] Under the same conditions, adding ethylenediaminetetraacetic (EDTA) as an organic additive allowed magnesite to be obtained at a temperature as low as 60 °C in 7 days.[12]

The cited investigations highlight the beneficial effects of chelating anions, such as carboxylate groups, for accelerating the MC[13] and possibly the precipitation of magnesite. These methods corroborate the theorized ability of some anions to stabilize the undercoordinated form of $Mg^{2+}$ in water solution, facilitating the precipitation of the anhydrous $MgCO_3$ phase and the further incorporation of anhydrous units in the precipitated phase.[14–17]

Recently, we employed microwave (MW) irradiation to drive the water-mediated carbonation reaction of brucite,[18] $Mg(OH)_2$, a representative Mg-bearing mineral which is the reactive component of widespread silicates such as serpentine, $Mg_3Si_2O_5(OH)_4$. Thanks to the strong coupling of electromagnetic waves in the GHz range with ionic species in solution, it was proven that MW irradiation allows for a substantial increment of the water-mediated MC reaction kinetics, enhancing both the dissolution and precipitation processes.[19] Notwithstanding the observed boosting of the MC, magnesite formation within a treatment time of 2 h was observed for temperatures higher than 190 °C.[18]

Here, we tested in parallel experiments of MW-assisted MC the effects of the addition of more than 20 additive anions, demonstrating experimentally that some of them give rise to a substantial catalytic effect, allowing for the direct precipitation of $MgCO_3$ starting from brucite at temperatures as low as 100 °C and achieving reaction completion in a few hours under partial pressure of $CO_2$ as low as 8 bar. We quantitatively investigated the precipitated phases by X-ray diffraction, electron microscopy, and Raman spectroscopy, determining the reaction yields. The mechanism underpinning this catalytic effect was explored by carrying out MC with progressively vanishing additive concentrations. We also investigated the possible benefits deriving from the adoption of MW and additive anions for the far less critical carbonation of portlandite, $Ca(OH)_2$. Identifying such MW-active MC catalyzers paves the way for a factual large-scale application of MW-assisted MC as a method of choice for CCUS.

## 2. Results and Discussion

### 2.1. Magnesite Precipitation

**Table 1** summarizes the results of the powder X-ray diffraction (PXRD) characterization of the products obtained in carbonation experiments of brucite with a subgroup of additives, whereas Table S1, Supporting Information, reports the results obtained with all selected additives. At 190 °C and $t_{dw} = 30$ min, and at 160 °C and $t_{dw} = 60$ min, brucite gives rise to a product composed of 100% of the MHCH hydromagnesite $[Mg_5(CO_3)_4(OH)_2{\cdot}4H_2O]$, with a yield reaching 81%. Under the same conditions, the majority of tested additive anions have a catalyzing effect, demonstrated by the presence of amounts higher than 1% of magnesite in the products. This is the case, e.g., of fumarate (FUM). **Figure 1** shows the comparison between PXRD patterns of pristine brucite and products of the MC of brucite without any additive and with FUM.

The action of FUM induces the presence of a small but detectable fraction (of the order of 1%, on the basis of the sensitivity of the technique) of magnesite, identified by the most intense peaks at $2\theta = 32.64°$ (104), 42.99° ($2\bar{1}3$), and 53.88° ($10\bar{8}$). The performance of FUM is even better at 160 °C and $t_{dw} = 60$ min, at which magnesite is recovered with a fraction of 8% (Table 1). Differently from FUM, other additives, such as formate (HCOO), malate (MAL), iodide (I), nitrate (NO3), and betaine (B), do not induce any presence of magnesite or any increment of magnesite fraction (Table S1). This group of additives can be termed *weak catalyzers* of magnesite precipitation. Similarly to FUM, other additives, such as acetate (CH3COO), oxalate (C2O4), lactic acid (LAC), betaine hydrochloride (BHC), and choline chloride (CHCL), allow to obtain magnesite with a fraction substantially higher than 1% (**Figure 2** and Table S1). This group of additives can be termed *medium catalyzers* of magnesite precipitation. However, in the case of C2O4, the presence of Mg-oxalate dihydrate in the precipitates was detected, making this additive not a proper catalyzer. It must also be noted that the carbonation yield in the presence of any of the aforementioned additives is always reduced with respect to that reached without additives (first two rows of Table 1 and Table S1).

A group of additives comprising phthalate (PHCOO), dihydrogen phosphate (H2PO4), hydrogen phosphate (HPO4), chloride (CL), and floride (F), does not show any catalyzing effect (Table S1). However, some of them have peculiar effects on the reaction that deserve a comment. PHCOO induces the precipitation of a pure hydromagnesite phase, as in the case of the absence of additives, but with a substantially reduced yield (81% with no additive, 22% with additive). Phosphates inhibit the precipitation of any carbonate phase and produce precipitates with complex composition, possibly represented by a mixture of Mg-phosphate hydrates.

Finally, additives such as malonate (MAO), succinate (SUC), tartrate (TAR), citrate (CIT), EDTA, hydrogen carbonate (HCO3), and sulfate (SO4), allow for the precipitation of pure or almost pure phases of magnesite at 190 °C and/or 160 °C. Therefore, they can be termed *strong catalyzers* (**Figure 3**a and **4**a).

Noteworthy, TAR and EDTA inhibit any precipitation in treatments at 190 °C but allow to obtain pure magnesite at 160 °C

**Table 1.** Weight percent of carbonate products (Br: unreacted brucite, H: hydromagnesite, M: magnesite) and maximum yields obtained in MW-assisted carbonation experiments ($T$: setpoint temperature; $t_{dw}$: dwelling time) of water slurries of brucite in the presence of equimolar amounts (or with multiple molar ratio as indicated in brackets in the first column) of selected additive anions.

| Additive | $T$ [°C] | $t_{dw}$ [min] | Br [%] | H [%] | M [%] | Yield [%] |
|---|---|---|---|---|---|---|
| None | 190 | 30 | – | 100 | – | 81 |
| | 160 | 60 | – | 100 | – | 78 |
| FUM | 190 | 30 | – | ≤99 | ≥1 | 68 |
| | 160 | 60 | 5 | 87 | 8 | 64 |
| MAO | 190 | 30 | – | – | 100 | 75 |
| | 160 | 60 | – | 16 | 84 | 36 |
| SUC | 190 | 30 | – | 43 | 57 | 91 |
| | 160 | 60 | – | 97 | 3 | 63 |
| CIT | 190 | 30 | – | – | 100 | 49 |
| | 160 | 60 | – | – | 100 | 36 |
| | 145 | 120 | – | – | 100 | 47 |
| | 145 | 60 | – | – | 100 | 49 |
| (×1.5) | 145 | 60 | – | – | 100 | 16 |
| | 130 | 60 | – | – | 100 | 50 |
| | 115 | 60 | – | – | 100 | 31 |
| (×0.75) | 115 | 60 | – | – | 100 | 46 |
| (×0.5) | 115 | 60 | – | – | 100 | 58 |
| | 115 | 120 | – | – | 100 | 36 |
| (×0.75) | 115 | 120 | – | – | 100 | 50 |
| (×0.5) | 115 | 120 | – | – | 100 | 62 |
| | 100 | 60 | – | – | 100 | 9 |
| (×0.75) | 100 | 60 | – | – | 100 | 32 |
| (×0.5) | 100 | 60 | – | – | 100 | 51 |
| | 100 | 120 | – | – | 100 | 13 |
| (×0.75) | 100 | 120 | – | – | 100 | 37 |
| (×0.5) | 100 | 120 | – | – | 100 | 53 |
| SO4 | 190 | 30 | – | 29 | 71 | 71 |
| | 160 | 30 | – | 98 | 2 | 70 |
| | 160 | 60 | – | 4 | 96 | 80 |
| | 145 | 60 | – | 91 | 9 | 71 |
| (×3) | 145 | 60 | – | 19 | 81 | 79 |
| | 145 | 120 | – | 43 | 57 | 82 |
| (×3) | 145 | 120 | – | – | 100 | 84 |
| (×3) | 130 | 60 | 6 | 82 | 12 | 74 |
| BHC | 190 | 30 | – | 92 | 8 | 28 |
| | 160 | 60 | – | ≤99 | ≥1 | 41 |
| CHCL | 190 | 30 | – | 96 | 4 | 70 |
| | 160 | 60 | – | 100 | – | 84 |

(Table S1). For HCO3, CIT, and SO4, we explored the effects of lower temperatures and different dwelling times and concentrations of the additive. HCO3 allows for the precipitation of

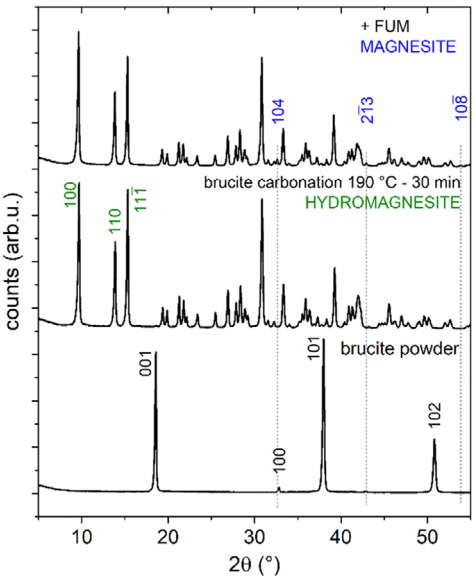


**Figure 1.** PXRD patterns collected on brucite pristine powder (lower pattern), precipitates of brucite carbonation at 190 °C and $t_{dw} = 30$ min (middle pattern, corresponding to hydromagnesite 100%), and precipitates of brucite carbonation at 190 °C and $t_{dw} = 30$ min with FUM in equimolar amounts as additive (upper pattern, corresponding to hydromagnesite 99% and magnesite 1%). Indexation of principal diffraction peaks is in accordance with the structures reported by references[24,36,45] for brucite, hydromagnesite, and magnesite, respectively.

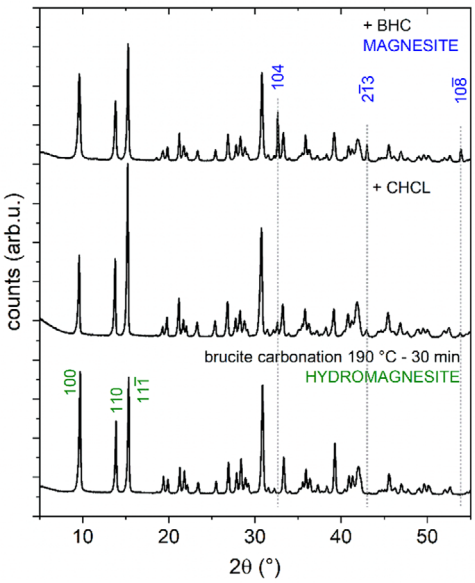


**Figure 2.** PXRD patterns collected on precipitates of brucite carbonation at 190 °C and $t_{dw} = 30$ min (lower pattern, corresponding to hydromagnesite 100%), and precipitates of brucite carbonation at 190 °C and $t_{dw} = 30$ min with CHCL in equimolar amounts as additive (middle pattern, corresponding to hydromagnesite 96% and magnesite 4%), and with BHC in equimolar amounts as additive (upper pattern, corresponding to hydromagnesite 92% and magnesite 8%).

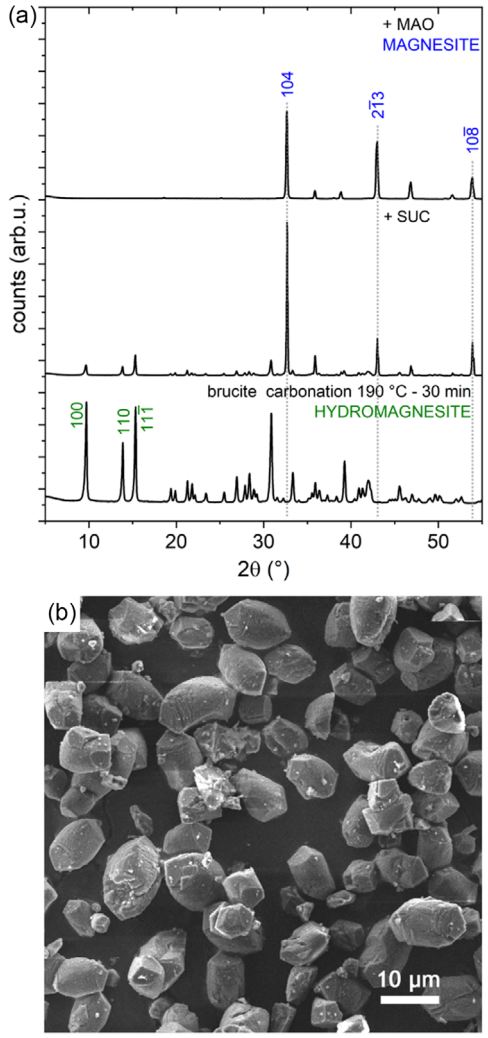


**Figure 3.** a) PXRD patterns of precipitates of brucite carbonation at 190 °C and $t_{dw} = 30$ min with MAO in equimolar amounts as additive (upper pattern, corresponding to magnesite 100%.); with SUC in equimolar amounts as additive (middle pattern, corresponding to hydromagnesite 57% and magnesite 43%), and no additive (lower pattern, corresponding to hydromagnesite 100%). b) SEM image of precipitates of brucite carbonation at 190 °C and $t_{dw} = 30$ min with MAO as additive.

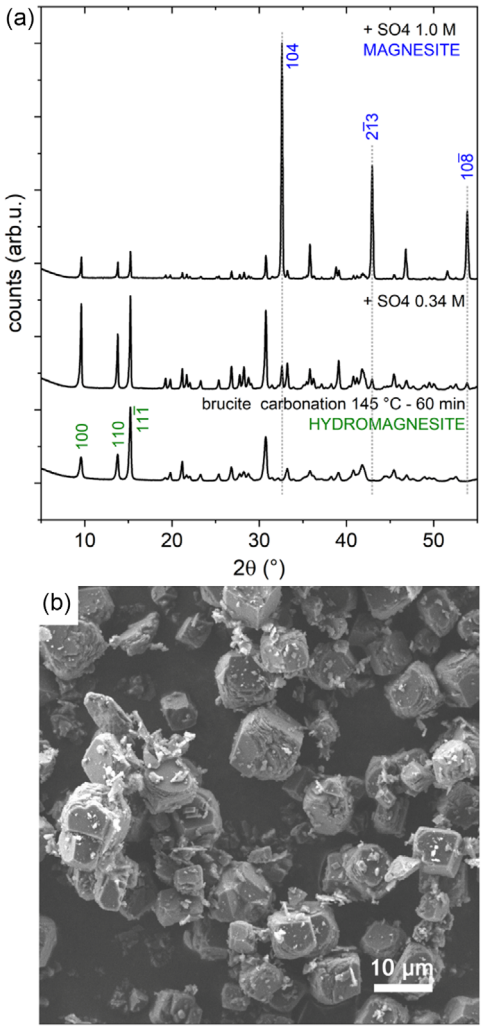


**Figure 4.** a) PXRD patterns collected on precipitates of brucite carbonation at 145 °C and $t_{dw} = 60$ min with SO4 1 M as additive (molar ratio SO4/Br = 3.0, upper pattern, corresponding to hydromagnesite 19% and magnesite 81%); with SO4 0.34 M (molar ratio SO4/Br = 1.0, middle pattern, corresponding to hydromagnesite 91% and magnesite 9%); and with no additive (lower pattern, corresponding to hydromagnesite 100%). b) SEM image of precipitates of brucite carbonation at 145 °C and $t_{dw} =$ 60 min with SO4 1 M as additive.

magnesite with high yield at temperatures as low as 145 °C. Similarly, SO4 allows to obtain a high fraction of magnesite in the precipitate with high yields for temperatures as low as 130 °C. For SO4, a positive effect of the increment of the additive concentration is apparent: e.g., at 145 °C and 60 min, by triplicating the additive concentration, the magnesite fraction increases from 9 to 81% (Figure 4a), and by prolonging the treatment to 120 min, a pure magnesite phase is obtained with a yield of 84% (Table 1). CIT was demonstrated to allow for the precipitation of a pure magnesite phase at temperatures as low as 100 °C (**Figure 5**a).

However, unlike SO4, beneficial effects on the precipitate yield are accomplished by diluting the additive. This can be promptly observed in the data reported in **Table 2** and plotted in **Figure 6**, where the yield of precipitation of pure magnesite increases both with $t_{dw}$ and Br/CIT molar ratio. Indeed, for CIT/Br = 1.5, no precipitation is observed within the whole range of explored reaction time, whereas magnesite yield reaches over 50% for CIT/Br = 0.5.

Fitting of the experimental data in Figure 6 was performed by applying the two-step Finke–Watzky (F–W) model.[20,21] Our choice of the F–W model started from the observation of an apparent sigmoidal trend of kinetic curves, evidencing the role played by induction time. The F−W two-step model consists of a slow, continuous nucleation (A → B, rate constant $k_1$) and a fast, autocatalytic growth (A + B → 2B, rate constant $k_2$). For the sake of simplicity, we consider the first step to consist

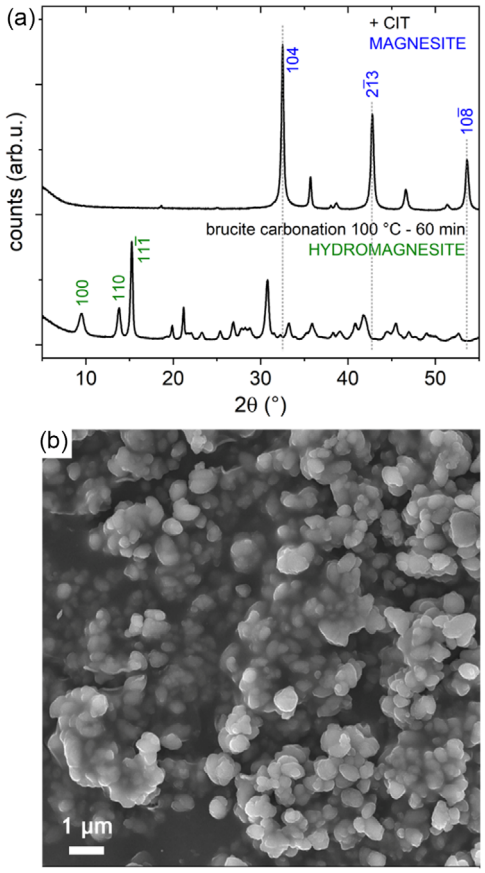


**Figure 5.** a) PXRD patterns collected on precipitates of brucite carbonation at 100 °C and $t_{dw} = 60$ min with CIT in equimolar amounts as an additive (upper pattern, corresponding to magnesite 100%); and with no additive (lower pattern, corresponding to hydromagnesite 100%). b) SEM image of precipitates of brucite carbonation at 100 °C and $t_{dw} =$ 60 min with CIT as additive.

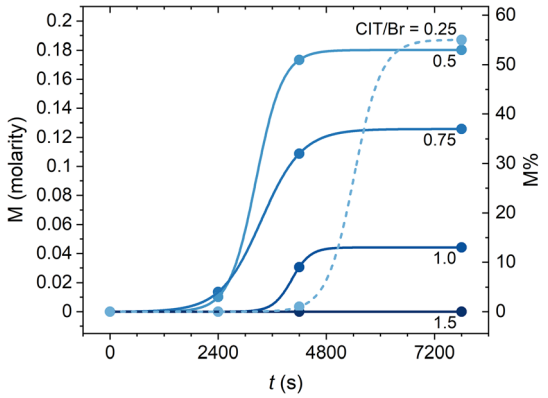


**Figure 6.** Magnesite molarity and yield as a function of reaction time ($0 < t < 600$ s: heating stage; $t > 600$ s: dwelling stage) and CIT/Br molar ratio in MW-assisted carbonation experiments of brucite slurries at a set-point temperature of 100 °C. Sigmoidal curves are obtained by fitting experimental data with the Finke–Watzky model. Best-fit parameters are listed in Table 2.

of the continuous slow nucleation of solid (s) magnesite due to the combination of aqueous $Mg^{2+}$ (aq, not chelated by CIT) and $CO_3^{2-}$ ions.

$$Mg^{2+}_{(aq)} + CO^{2-}_{3,(aq)} \xrightarrow{k_1} MgCO_{3,(s)} \quad (1)$$

In fact, this step comprises the dissolution of brucite.

$$Mg(OH)_{2,(s)} + CO_{2,(aq)} \rightarrow Mg^{2+}_{(aq)} + CO^{2-}_{2,(aq)} + H_2O \quad (2)$$

and the chelation of part of Mg ions.

$$Mg^{2+}_{(aq)} + CIT^{3-}_{(aq)} \rightarrow [Mg^{2+}: CIT^{3-}]_{(aq)} \quad (3)$$

The second step consists of the autocatalytic growth of magnesite due to the incorporation of $Mg^{2+}$ and $CO_3^{2-}$ ions.

$$Mg^{2+}_{(aq)} + CO^{2-}_{2,(aq)} + MgCO_{3,(s)} \xrightarrow{k_2} 2MgCO_{3,(s)} \quad (4)$$

The overall reaction rate for magnesite (M) precipitation is regulated by the rate constants $k_1$ and $k_2$ and can be expressed as

**Table 2.** Carbonation yield in terms of magnesite ($M_y$) and nesquehonite ($N_y$) obtained in MW-assisted carbonation experiments at 100 °C and different dwelling times of water slurries of brucite in the presence of CIT with different molar ratios to brucite slurry. The weight fraction of residual brucite within the precipitates is indicated with Br. The last three columns report kinetic parameters extracted by interpolating experimental data with the Finke–Watzky sigmoidal curve. Data are affected by an uncertainty of 10–15% deriving from the mass and volume measurements of reactants and water.

| CIT/Br | $t_{dw} = 30$ min | | | 60 min | | | 120 min | | | $[Mg_{(aq)}{}^{2+}]_0$ [mol $L^{-1}$] | $k_1$ [$s^{-1}$] | $k_2$ [$mol^{-1}$ L $s^{-1}$] |
|---|---|---|---|---|---|---|---|---|---|---|---|---|
| | Br [%] | $N_y$ [%] | $M_y$ [%] | Br [%] | $N_y$ [%] | $M_y$ [%] | Br [%] | $N_y$ [%] | $M_y$ [%] | | | |
| 1.5 | – | – | – | – | – | – | – | – | – | – | – | – |
| 1.0 | – | – | – | – | – | 9 | – | – | 13 | 0.044 | $1.8 \times 10^{-11}$ | 0.11 |
| 0.75 | 13 | – | 4 | – | – | 32 | – | – | 37 | 0.13 | $1.4 \times 10^{-6}$ | 0.017 |
| 0.50 | 79 | – | 3 | – | – | 51 | – | – | 53 | 0.18 | $6.3 \times 10^{-8}$ | 0.019 |
| 0.25 | 2 | 45 | – | 3 | 39 | 1 | – | – | 55 | 0.19 | $6.4 \times 10^{-11}$ | 0.018 |
| 0.0 | 42% Br + 58% H (carb. yield: 44%) | | | | – | | | – | | | – | |

$$\frac{d[M]_t}{dt} = k_1[Mg^{2+}_{(aq)}]_t + k_2[Mg^{2+}_{(aq)}]_t[M]_t \quad (5)$$

Integration of Equation (5) brings to the sigmoidal rate law for magnesite precipitation. $[X]_t$ represents the concentration (mol $L^{-1}$) of the species X at time $t$. For simplicity, we can assume that initially $[M]_0 = 0$ and that the sum $[Mg^{2+}_{(aq)}]_t + [M]_t$ at all times is not equal to the initial brucite concentration (0.34 mol $L^{-1}$) but to the maximum concentration of aqueous not-chelated Mg-ions, which we refer to as $[Mg^{2+}_{(aq)}]_0$.

As can be seen from the parameters extracted from the fitting procedure (Table 2), the value of $[Mg^{2+}_{(aq)}]_0$ corresponds to the late-time magnesite yield. If CIT/Br $\geq 1$, Mg-ions are not in the condition of combining with $CO_3^{2-}$ and precipitation is substantially inhibited: for CIT/Br = 1.5, we observe no evidence of precipitates within a reaction time of 2 h. For CIT/Br = 1.0, the nucleation rate is vanishingly low, and the forming magnesite is substantially the result of an incorporation process (reaction (4)). If CIT/Br $< 1$, Mg-ions are in the condition of precipitating, with a magnesite nucleation rate ($k_1$) of the order of $10^{-6}$ $s^{-1}$ and a growth rate ($k_2$) of the order of $10^{-2}$ $mol^{-1}$ L $s^{-1}$, reaching an overall yield of the order of 50% for CIT/Br = 0.5. If CIT/Br $< 0.5$, the precipitation mechanism changes, leading to the formation of nesquehonite instead of magnesite.

It is interesting to note that almost pure magnesite samples obtained with MAO, SO4, and CIT present substantial differences with respect to their crystallinity and morphology. The PXRD pattern of magnesite precipitated from CIT (Figure 5a) presents peaks with a substantially larger width with respect to those in the patterns collected from MAO and SO4 (Figure 3a and 4a, respectively), indicating lower crystallinity. In accordance with this, the scanning electron microscopy (SEM) image reported in Figure 5b shows subeuhedral crystallites with an average size below 1 μm, indicating a cooperative effect given by the possible formation of early-stage amorphous phases[22] and growth inhibition induced by the citrate.[23] On the contrary, samples shown in SEM images of magnesite obtained from MAO (Figure 3b) and SO4 (Figure 4b) show well-defined crystallites with an average size of 10 μm. Interestingly, magnesite crystallites precipitated from SO4 solutions present a rhombohedral morphology similar to that obtained without additives,[18,24] while those precipitated from MAO show an ellipsoidal shape.

We have performed Raman spectroscopy analysis to gain deeper insights into these almost pure magnesite products obtained by the MAO, SO4, and CIT additives (**Figure 7**). The three Raman spectra display the evident peaks of the carbonate symmetric stretching (1090 $cm^{-1}$) and bending (732 $cm^{-1}$). Furthermore, for the sample treated with MAO, we also observed the characteristic OH stretching (3647 $cm^{-1}$) attributed to some residual unreacted brucite. The outcomes of Raman spectroscopy confirm the formation of magnesite, in agreement with PXRD. We do not observe in the OH stretching region of the Raman spectra any of the broad and structured features that are characteristic of hydromagnesite and nesquehonite.[18] This is due to the low quantity of these phases in the sample.

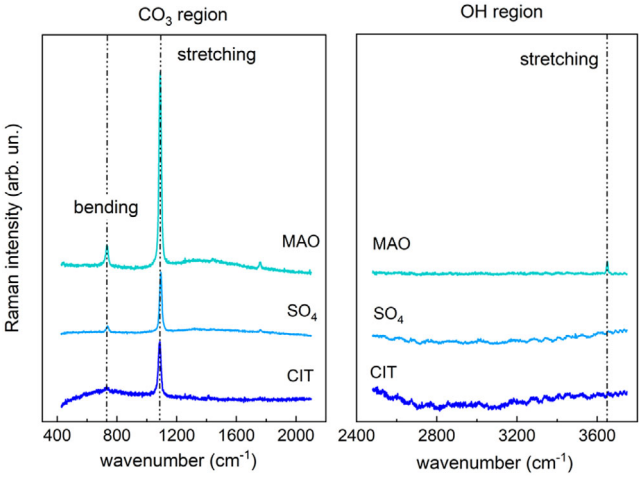


**Figure 7.** Raman spectra of the carbonation products obtained from brucite samples treated with different additives (MAO, SO4, CIT as described in Figure 3–5, respectively). The excitation laser was 633 nm for all the acquired spectra.

## 2.2. Calcite Precipitation

The precipitation of calcium carbonates by carbonation of portlandite is a far more rapid process than the carbonation of brucite, and the anhydrous phase of calcite is obtained even at room temperature after a few minutes. For this reason, the advantages of adopting MW heating and additive anions could be marginal. However, contrary to this expectation, **Figure 8**a demonstrates that by maximizing MW exposure in carbonation experiments performed without a vial rack (see Section 4), the carbonation rate of portlandite is almost doubled by MW heating compared to thermal heating.

We selected some of the additives listed in Table 1 to test their effect as catalyzers in parallel carbonation experiments of portlandite performed in a vial rack. **Table 3** summarizes the results of the PXRD characterization of the products obtained. At 35 °C and $t_{dw}$ = 5 min, portlandite gives rise to a product composed of 22% calcite, with a residue of 78% of unreacted portlandite. Some additives giving positive results for the carbonation of brucite are also observed to be able to increase the fraction of calcite. This is the case of CH3COO and NO3 that increment the calcite fraction from 22 to 45 and 49, respectively (**Figure 9**a). Similarly to the case of brucite, the presence of the additive anion brings about a decrease in the carbonation yield. Contrary to what was observed with brucite, CIT has a negative effect on the precipitation of calcite,[25] reducing the fraction of this product to 12%, with an overall carbonation yield as low as 4% (Figure 9a and Table 3). TAR apparently allows to obtain an almost pure crystalline phase of calcite; however, the intensity of the PXRD pattern is relatively low, due to the presence of a significant fraction of an amorphous phase.

The SEM micrograph reported in Figure 8b, corresponding to an almost pure sample of calcite, shows the presence of submicrometric elongated crystallites grouped in cauliflower-shaped clusters.[26,27] This morphology is partially preserved in calcite

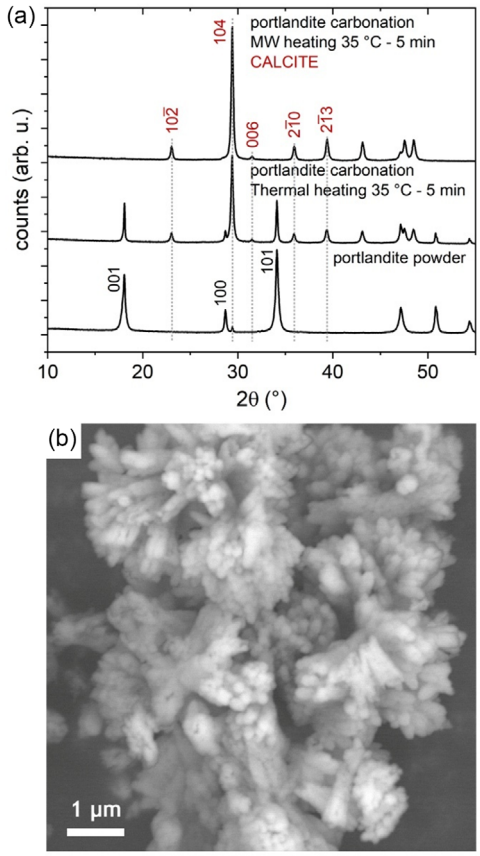


**Figure 8.** a) PXRD patterns collected on portlandite pristine powder (lower pattern), precipitates of portlandite carbonation with thermal heating at 35 °C and $t_{dw} = 5$ min (middle pattern, corresponding to calcite 64% and residual portlandite 36%), and precipitates of portlandite carbonation at 35 °C and $t_{dw} = 5$ min with MW heating (upper pattern, corresponding to calcite 98% and residual portlandite 2%). Indexation of principal diffraction peaks is in accordance with the structures reported by references[24,37] for portlandite and calcite, respectively. The 104 peak of calcite visible in the lower pattern is due to the spontaneous carbonation of portlandite powder in the air. b) SEM image of precipitates of portlandite carbonation with MW heating at 35 °C and $t_{dw} = 5$ min.

**Table 3.** Weight percent of carbonate products (Po: unreacted portlandite, C: calcite) and maximum yields obtained in MW-assisted carbonation experiments at 35 °C and $t_{dw} = 5$ min of water slurries of portlandite in the presence of equimolar amounts of additive anions.

| Additive | Po [%] | C [%] | Yield [%] |
|---|---|---|---|
| None | 78 | 22 | 16 |
| CH3COO | 55 | 45 | 31 |
| CIT | 88 | 12 | 4 |
| TAR | 4 | 96 | Presence of amorphous BCC |
| NO3 | 51 | 49 | 34 |

precipitates obtained from TAR solutions (SEM image in Figure 9b), even though a fine-grained amorphous phase in the background makes it less defined.

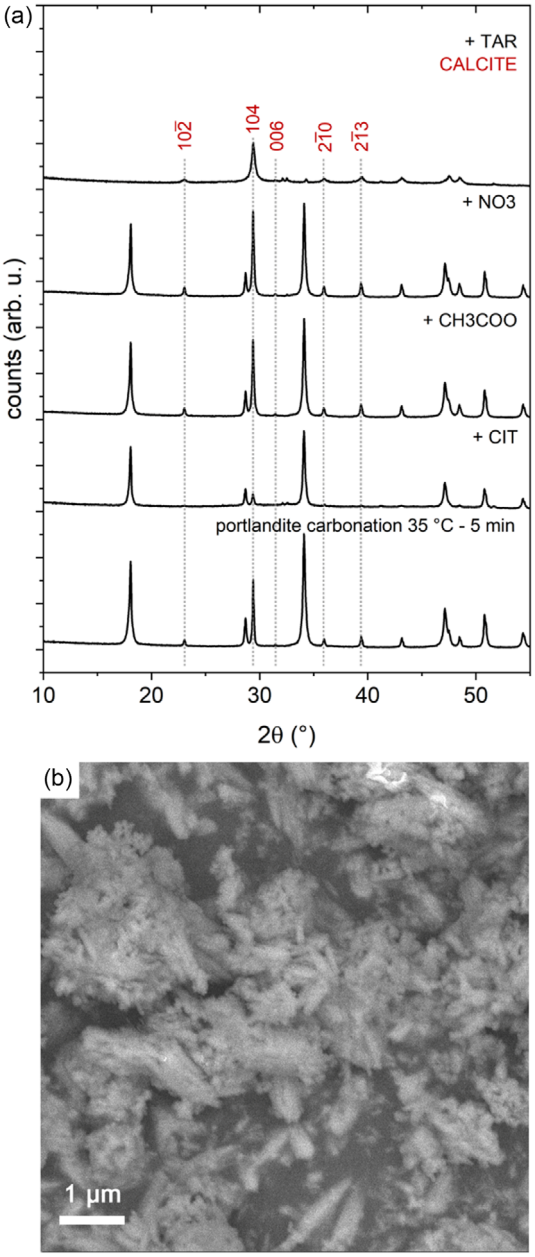


**Figure 9.** a) PXRD patterns collected on precipitates of portlandite carbonation at 35 °C and $t_{dw} = 5$ min with, from top to bottom, TAR in equimolar amounts as an additive (corresponding to calcite 96% and residual portlandite 4%); with NO3 as an additive (corresponding to calcite 49% and residual portlandite 51%); with CH3COO as an additive (corresponding to calcite 45% and residual portlandite 55%); with CIT as an additive (corresponding to calcite 12% and residual portlandite 88%), and with no additive (corresponding to calcite 22% and residual portlandite 78%). b) SEM image of precipitates of portlandite carbonation at 35 °C and $t_{dw} = 5$ min with TAR as additive.

We have investigated by using Raman spectroscopy the pure calcite precipitate obtained from the carbonation reaction of portlandite without a rack (Figure 8) and in the presence of TAR as an additive (Figure 9).

The Raman spectrum reported in **Figure 10** of the "no rack" sample shows very sharp peaks characteristic of calcite, specifically the symmetric stretching (1081) and bending (710 $cm^{-1}$) vibrations. For the TAR sample, we observe the carbonate symmetric stretching (1081) and bending (710 $cm^{-1}$) peaks, but additional intense peaks are observed that can be attributed to basic calcium carbonate (BCC). This is apparent from the comparison of the Raman spectral pattern in the 600–2100 $cm^{-1}$ region of Figure 10 with respect to the Raman spectrum of BCC reported in the literature.[28] Interestingly, when changing the excitation wavelength to 473 nm, the Raman spectrum of the TAR sample evolves and the intensity of the main carbonate peak (1081 $cm^{-1}$) is enhanced compared to the other Raman features. This behaviour reflects the different wavelength dependence of the Raman cross-section of different phases that are present in the sample. The results from Raman spectroscopy confirm for the "no rack" sample the formation of pure calcite (no presence of peaks in the OH region and the presence of the carbonate stretching and bending markers) and suggest for the TAR sample the formation of BCC. This latter observation complements the PXRD results reported in Figure 9a for the same additive since diffraction data do not reveal the presence of the BCC phase probably because of its relatively low cross-section for X-ray diffraction and its occurrence in an amorphous state.[29,30]

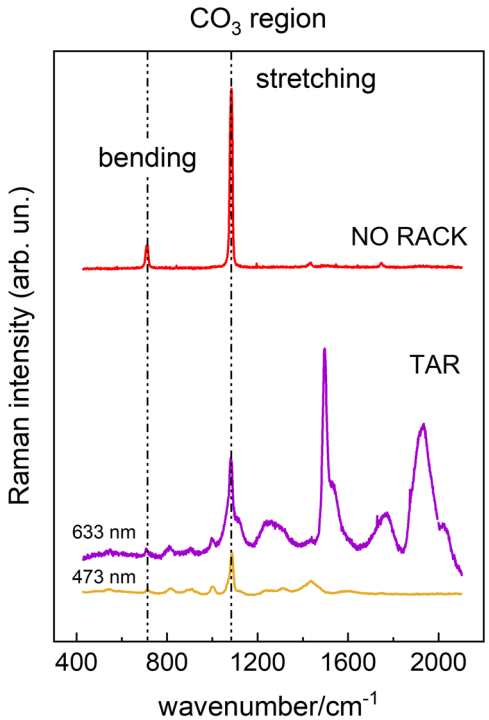


**Figure 10.** Raman spectra of the carbonation products obtained from $Ca(OH)_2$ slurries with no additive and without the attenuation barrier given by the base load (NO RACK) and with equimolar amounts of TAR additive. The excitation laser was 633 nm for the acquisition of red- and purple-line spectra, whereas it was 473 nm for the light-brown spectrum.

### 2.3. Action and Classification of Catalyzers for MC

It is recognized that the fundamental step for $MgCO_3$ nucleation is represented by the activation of $Mg^{2+}$ dehydration.[17] In our carbonation experiments, hydrated $Mg^{2+}$ ions form as a consequence of a dissolution step of brucite, facilitated by the acidic environment created by slightly pressurizing the $CO_2/N_2$ mixture (see Experimental Section).

$$Mg(OH)_{2,(s)} + CO_{2,(aq)} + 5H_2O \rightarrow Mg(H_2O)_6^{2+} + CO_{2,(aq)}^{2-} \quad (6)$$

In the second step, the stability of the hexahydrated complex and energy barriers regulate the spontaneity and rapidity of its combination with the carbonate anion to form solid magnesite or incorporation of $Mg^{2+}$ into the magnesite crystal lattice.

$$Mg(H_2O)_6^{2+} + CO_{2,(aq)}^{2-} \rightarrow MgCO_{3,(s)} + 6H_2O \quad (7)$$

This latter reaction requires a temperature higher than 190 °C, which can be reached either by thermal[31] or MW-aided heating.[18] A strategy to lower this temperature consists of perturbing the stability of the hexahydrated complex by introducing proper additive anions, $X^{n-}$, which activate the metal cation dehydration. In this framework, the simultaneous accomplishment of three criteria was suggested to identify successful additives promoting the direct nucleation of $MgCO_3$. These criteria are 1) the formation of a stable contact-ion-pair (CIP) $Mg^{2+}\cdots X^{n-}$, i.e., with the counterion occupying the first hydration shell of $Mg^{2+}$, which are not competitive with $Mg^{2+}\cdots CO_3^{2-}$; 2) the stabilization of the undercoordinated $Mg(H_2O)_5^{2+}$ complex in a solvent-share-ion pair (SShIP), i.e., with the counterion occupying the second hydration shell of $Mg^{2+}$, displaying a vacant site to be occupied with $CO_3^{2-}$; and 3) the stabilization of the $Mg(H_2O)_{3\text{-}4}^{2+}$ complex in a CIP with the anion.[14]

On this basis, key thermodynamic parameters are represented by the free energy difference $\Delta G_{i\rightarrow j}$ and free energy barrier $\Delta^{\ddagger}G_{i\rightarrow j}$ between two coordination states $i$ and $j$. Theoretical studies show that while $\Delta G_{i\rightarrow j}$ can be lowered by exploiting the interaction with proper additive anions, the energy barrier for dehydration in a neutral environment is significant, ranging from 0.41 (40) to 0.67 eV (65 kJ $mol^{-1}$).[14,17] This suggests that the catalytic effect of an additive anion manifests itself through the lowering of this barrier. In this respect, MW radiation, by coupling directly with electrolytes and promoting their mobilization, represents a physical means to facilitate the passing of this barrier.

The solution additives that were assessed by Toroz et al.[14] as theoretically able to promote $Mg^{2+}$ dehydration based on the aforementioned three criteria are CIT, C2O4, SO4, MAL, H2PO4, and aminophenolate ($C_5H_4ONH_2^-$). On the basis of our experimental results (Table 1 and S1, Supporting Information), which include the investigation of most of the anions involved in this theoretical study, we can conclude that CIT and SO4 can be considered as effective promoters of $Mg^{2+}$ dehydration and are strong catalyzers of magnesite precipitation. C2O4 was assessed as an effective promoter of magnesite precipitation; however, the simultaneous formation of insoluble Mg oxalates hinders the possibility of counting this additive as a proper catalyzer. On the contrary, MAL was demonstrated to

have only a weak effect on promoting the precipitation of magnesite, while H2PO4 induced no precipitation of magnesite. Finally, we did not test aminophenol. However, we demonstrated the efficacy of TAR and HCO3, which were not mentioned among those fulfilling the three criteria, and we identified other promising catalyzers for magnesite precipitation, namely MAO, SUC, and EDTA.

On the basis of this comparison, the simultaneous fulfilment of the three criteria adopted for establishing the ability of an additive to promote $Mg^{2+}$ dehydration appears, with some exceptions, as sufficient for establishing the catalytic action of a chemical species.

It must be noted that, even though the theoretical study refers to room temperature and 1 bar pressure conditions, each catalyzer presents a specific temperature limit below which it is no longer able to promote magnesite precipitation. In this respect, direct magnesite precipitation was never observed at room temperature within a 2-h timelapse. The addition of strong inorganic catalyzers such as SO4 and HCO3 allows for the obtaining of large magnesite fractions at temperatures as low as 130 °C. Below this limit, hydromagnesite becomes the favourite carbonate phase. The organic additive CIT allows to obtain pure magnesite precipitates at temperatures as low as 100 °C. The accomplishment of these temperature levels and the reduced time needed to complete the reaction represent notable targets, opening the possibility of performing water-mediated MC at large scales, in continuous, and under near-to-ambient-pressure conditions.

Besides this characteristic temperature limit for successful magnesite precipitation, the group of catalyzers can be divided into two categories, depending on the effect of the increment of their concentration on the yield of carbonation. Following recent results of MC of olivine,[32] the increment of the concentration of SO4 brings beneficial effects in terms of increase of magnesite fraction in the precipitates and yield of the carbonation reaction of brucite (Table 1 and Figure 4). On the contrary, high concentrations of CIT inhibit the precipitation of carbonates. In this case, a trade-off must be reached to allow for adequate coordination of the hydrated $Mg^{2+}$ ions without inhibiting their combination with $CO_3^{2-}$ (Table 1 and Figures 5 and 6). Indeed, the kinetics of magnesite precipitation at 100 °C is characterized by relevant induction periods, while the growth rate is substantially invariant with CIT concentration (Table 2 and Figure 6). We attribute this behaviour to the chelating action of CIT, which, unlike SO4 or other inorganic additives, can dissolve magnesite. We note that parallel experiments performed under the same conditions without $CO_2$ did not allow the brucite to dissolve. This substantiates a more critical competition between the $Mg^{2+}...CO_3^{2-}$ and $Mg^{2+}...CIT^{3-}$ CIPs with respect to what is observed theoretically. Notwithstanding this competition, the kinetic curve in Figure 6 with $CIT/Br = 1.0$ reveals clearly that the carbonation reaction consists of two steps: the first step is the brucite dissolution with the formation of the $Mg^{2+}\cdots CIT^{3-}$ complex (absence of precipitates at $t < 2400$ s), and the second step is the MW-induced decomplexation[33] with precipitation of $MgCO_3$. However, for very dilute solutions of CIT ($CIT/Br < 0.5$), an intermediate step of nucleation of nesquehonite is observed (Table 2). This is impressive because nesquehonite is unstable at 100 °C, transforming spontaneously to hydromagnesite starting from 55 °C.[18] Indeed, hydromagnesite is the product obtained without additives (last row of Table 2). This result reveals that CIT can inhibit the water-mediated transformation of nesquehonite into hydromagnesite.[34]

$$\mathrm{Mg(CO)_3 \cdot 3H_2O_{(s)} + CO_{2,(aq)}} \rightarrow \frac{1}{5}\mathrm{Mg_5(CO_3)_4(OH)_2 \cdot 4H_2O_{(s)}} + \frac{1}{5}\mathrm{CO_2} + 2\mathrm{H_2O} \quad (8)$$

This inhibition reveals that reaction (8) occurs through a dissolution–precipitation mechanism; otherwise, in the case of a direct solid-solid transition, hydromagnesite formation would be independent of the presence of a solution additive. The presence of this intermediate step can be considered as the basis of the reincrement of the induction period for magnesite precipitation of carbonation reactions observed for $CIT/Br < 0.5$ (Table 2 and Figure 6).

We have some indications that TAR and EDTA follow a similar behaviour as CIT, being both strong chelants, as evidenced by the absence of precipitates and low yields obtained in some of the tests listed in Table S1, Supporting Information.

Beneficial effects of CIT were recently observed by Miller et al. for the MC at 50 °C for up to 90 h at 90 bar $CO_2$ of forsterite.[35] Even though at 50 °C nesquehonite is the expected Mg carbonate, the very prolonged carbonation time did not produce any detectable amount of hydromagnesite, and, in accordance with our observations, the fraction of forming nesquehonite decreases with increasing CIT concentration.

Carbonation of portlandite presents substantial differences with respect to brucite, deriving both from the different structural properties and solubilities of the two minerals and from differences in the coordination chemistry of $Ca^{2+}$ and $Mg^{2+}$. Indeed, the much higher solubility of portlandite gives rise to alkaline slurries having an enhanced capability to absorb $CO_2$. The higher size of $Ca^{2+}$ with respect to $Mg^{2+}$ impacts the basal-plane lattice parameters and the spacing between octahedral layers, being expanded by 13.7% and 2.1%, respectively,[36,37] and making the mineral more prone to intercalate water.[38] This property was claimed to have a clear role in carbonation reaction, and we can specify that this may be at the basis of the enhancement of the carbonation kinetics produced by MW irradiation (Figure 8) since the absorption of MW by water molecules intercalated in mineral grains can be responsible for an expansion of the octahedral layers, facilitating further water intercalation up to the exfoliation and then increment of the surface/volume ratio of the mineral phase.

More elusive is the dehydration step of $Ca^{2+}$ for promoting $CaCO_3$ precipitation.[17,39] In fact, $Ca^{2+}$ has no stable pentacoordinate geometry, rather, it presents a near-degeneracy of the hexa- and hepta-coordinate geometry, and, at neutral pH, a stable minimum is observed for octa-coordinate geometry.[40] This does not signify that additive anions cannot stabilize the undercoordinated geometry for $Ca^{2+}$. Indeed, we actually verified that a substantial effect in terms of yield of carbonation reaction could be accomplished with a group of additives, allowing for the assessment of a catalyzing effect (see e.g., the case of CH3COO in Table 3). Similar to the case of $Mg^{2+}$, equimolar quantities of CIT substantially inhibit the precipitation of carbonates.

It is worth noting that the tested additive anions are almost all naturally occurring substances that might reach a significant concentration in soils and subsurface waters, thus influencing the speciation of carbonates in the environment. This is the case, e.g., of carboxylates, since the Krebs cycle comprises the biosynthesis of CIT, MAL, and SUC.[41] Another anion of particular relevance is SO4, both due to its abundance in nature and to the heated debate regarding its role as an inhibitor or accelerator of the Mg-carbonate precipitation.[42]

## 3. Conclusion

MC of brucite and portlandite water slurries was carried out under controlled temperature, pressure, and treatment time by providing MW irradiation in the presence of additive anions comprising a family of more than 20 chemical species within the classes of carboxylate, inorganic, and ammonium salts. Our results indicate that a catalytic approach to magnesite and calcite precipitation is feasible. This conclusion is drawn on the basis of the following observations: 1) Without additives, brucite direct conversion into magnesite is obtained at a temperature higher than 200 °C; a subgroup of additives, which we refer to as strong catalyzers, such as MAO, SUC, TAR, CIT, EDTA, HCO3, and SO4, allows to obtain the complete conversion of brucite into magnesite within times as short as 1 h and at temperatures as low as 100 °C; 2) Without additives, portlandite conversion into calcite is obtained at temperatures as low as 35 °C; however, MW irradiation allows to almost double the conversion rate; a subgroup of additives, such as CH3COO, TAR, and NO3, allows to further augment the yield of portlandite conversion into calcite within times as short as 5 min. Depending on the specificity of the ion pairing between the additive and the Mg- and Ca-cations, the increment of the concentration of the anion can improve or worsen the reaction yield. Chelating additives such as citrate promote magnesite precipitation at low temperatures and low concentrations even though with an increment of the induction time; at high concentrations, carbonate precipitation is inhibited. On the contrary, other active additives such as sulfate improve their catalytic activity as a consequence of an increment of their concentration. Since all equilibria of pairing, chelation and dechelation, involve ionic species, MW irradiation accomplishes a specific energisation of electrolytes, allowing for overtaking the energy barrier for dehydration of the metal ion, boosting their catalytic activity.

This study has an immediate impact on the development of MC using not only solid mineral waste as a source of Mg and Ca but also seawater and brines, containing Mg- and Ca-ions potentially available for carbonate precipitation but coexisting with other electrolytes.[8]

## 4. Experimental Section

Brucite (Br, Sigma-Aldrich BioUltra ≥99.0%) and portlandite (Po, ACS reagent >95.0%) slurries with a concentration of 0.34 M were prepared by dispersing the powder in deionized water with the aid of an ultrasound bath. Tested additives (all provided by Sigma-Aldrich) were chosen based on the database provided by Toroz et al.[14] avoiding expensive and environmentally hazardous compounds, namely (acronym in brackets): 1) carboxylic acids and potassium or sodium salts of mono-, di-, tri-, and tetra-carboxylic acids: lactic acid, $C_3H_6O_3$ (LAC), K-formate, $HCOO^-$ (HCOO), K-acetate, $CH_3COO^-$ (CH3COO), K-hydrogen phthalate, $C_8H_5O_4^-$ (PHCOO), $K_2$-oxalate, $C_2O_4^{2-}$ (C2O4), $K_2$-fumarate, $C_4H_2O_4^{2-}$ (FUM), $K_2$-malate, $C_4H_4O_5^{2-}$ (MAL), $K_2$-malonate, $C_3H_2O_4^{2-}$ (MAO), $K_2$-succinate, $C_4H_4O_4^{2-}$ (SUC), $K_2$-DL-tartrate, $C_4H_4O_6^{2-}$ (TAR), $K_3$-citrate, $C_6H_6O_7^{3-}$ (CIT), and $Na_4$-ethylenediamminotetraacetate, $C_{10}H_{12}N_2O_8^{4-}$ (EDTA); 2) inorganic salts: Na-hydrogen carbonate, $HCO_3^-$ (HCO3), K-dihydrogen phosphate, $H_2PO_4^-$ (H2PO4), $K_2$-hydrogen phosphate, $HPO_4^{2-}$ (HPO4), K-iodide, $I^-$ (I), $Na_2$-sulphate, $SO_4^{2-}$ (SO4), K-chloride, $Cl^-$ (CL), Na-fluoride, $F^-$ (F), K-nitrate, $NO_3^-$ (NO3); and 3) ammonium salts: betaine, $C_5H_9NO_2$ (B), betaine hydrochloride, $C_5H_{10}NO_2Cl$ (BHC), choline chloride, $C_5H_{10}NOCl$ (CHCL).

MCs were carried out in a MW reactor (SynthWave, Milestone) constituted by a 900-mL teflon-lined cylindrical resonant cavity equipped with a 1500 W magnetron. The MW antenna was placed at the base of the reactor (diameter 8.0 cm) and emits radiation axially to it.

*Carbonation of Brucite Slurries*: The reactor was filled with 200 mL of tap water (base load, in which the temperature gauge is immersed). The free volume of the cavity was used to insert a rack hosting up to 15 glass vials of volume 16 mL filled with 5.0 mL of brucite slurry and an equimolar quantity (if not stated differently) of the chosen additive. Each vial was stirred during the carbonation treatment with the aid of a built-in magnetic stirrer. The reactor was filled at room temperature with 8 bar of $CO_2$ (99.995%) and 6 bar of $N_2$ (99.999%), as measured by a built-in pressure gauge, and MW irradiation started for 10 min to reach with a linear rate the setpoint temperature (within the range 85–190 °C, *heating stage*). The setpoint temperature was maintained for a period of 30–120 min (*dwelling stage*). Irradiated energy was recorded throughout the treatment period. After termination of the dwelling stage, the reactor was cooled down to 35 °C by fluxing water at 8 °C provided by a chiller through its jacket. After that, the reactor was depressurized and opened to retrieve the products from the test tubes.

*Carbonation of Portlandite Slurries*: Due to the much higher reactivity of portlandite, MW irradiation started for 5 min under only 6 bar $N_2$, to reach with a linear rate the setpoint temperature of 35 °C. The setpoint temperature was maintained for a period of 5 min, and then 8 bar $CO_2$ was injected within a few seconds. The dwelling stage was maintained for 5 min, and then, the reactor was depressurized and opened to retrieve the products from the test tubes.

Since for MC of portlandite, the required dwelling stage was within 10 min and the setpoint temperature below 60 °C, the used apparatus was also suitable for carrying out isothermal treatment without the MW irradiation, allowing for a precise comparison of results obtained in carbonation experiments carried out under the same conditions but with a different heating method. This opportunity was achieved by starting the treatment with the reactor content (with or without a vial rack) and its jacket at room temperature. The filled reactor (pressurized only with $N_2$) was heated by MW irradiation at a temperature higher than the setpoint (for reaching a setpoint temperature of 35 °C, it was heated to 60 °C in 5 min), ensuring that the chiller flux was inactive. Then, irradiation was stopped, and the reactor content and external jacket were allowed to reach thermal equilibrium. Thanks to the relatively high heat capacity of the reactor-jacket system, at near thermal equilibrium the temperature was maintained for a long period, allowing for introducing the required amount of $CO_2$ and carrying out the carbonation treatment under isothermal conditions without the aid of MW irradiation.

The contents of the test tubes or reactor vessel after extraction were centrifuged, and the precipitated phase was separated from the supernatant solution, exsiccated in rotavapor, and analysed by PXRD and Raman spectroscopy for the qualitative and quantitative analysis of crystalline phases. PXRD of the solid products was performed with a Bragg-Brentano geometry X'Pert Pro Diffractometer (Malvern Panalytical), using Cu Kα radiation (1.5417 Å, 40 kV and 40 mA), and a divergence slit of 1/2°. The powder samples were back-loaded on a flat sample holder, and PXRD patterns were collected over a 2θ angular range of 5°–80°, with 0.0167°/step and a counting time of 90 s/step. Qualitative analyses were preliminary done employing the *Match!* software, whereas the phase amounts

(expressed in $\%_{w/w}$ throughout the paper) were evaluated from PXRD patterns through the full profile Rietveld Refinement Method,[43] implemented in GSAS software, and with EXPGUI as a graphical interface.[44] For the same carbonation experiment, weight percents were observed to have variability within $\pm 1\%$ whereas yields can vary up to $\pm 10\%$.

The micro-Raman measurements were carried out with the SOL-Nikon instrument using a 40× objective (0.75 NA, laser spot size about 3 μm), and the 633/473 nm excitation provided by a He-Ne and solid-state laser, respectively. Before measurements, the sample powder was gently pressed on a microscope glass slide. For each different point on the powder sample, the laser focusing procedure was repeated before collecting the Raman spectra. The different points on the sample were randomly selected within a zone of a few millimetres in diameter. For each sample in powder form, several spectra were collected by focusing the laser on different points of the sample. A negligible variation from point to point was observed, and the reported spectra can be considered representative of each sample.

A representative fraction of the obtained products was characterized by SEM (Gemini 500, Zeiss) equipped with a Quantax energy dispersive X-ray spectroscopy (Bruker) microanalysis system to characterize the grain morphology and composition of the obtained products.

*Assessment of the Catalyzing Effect of Additive Anions*: On the basis of previous studies of carbonation of brucite performed with this methodology with no additive,[18] a setpoint temperature of 190 °C represented the threshold beyond which magnesite amounts in the products give rise to a detectable signal in PXRD patterns (expressed by a fraction $\geq 1\%$). Therefore, it was established that an additive anion has a catalyzing effect if a detectable PXRD signal of the magnesite diffraction peaks was present in the products obtained at a temperature of 190 °C and a dwelling time $t_{dw} = 30$ min. The relative efficacy of the different catalyzers was then assessed by a second essay performed at 160 °C for 60 min. For a selected group of additives, the lowest setpoint temperature at which magnesite can be detected in the products within $t_{dw} \leq 60$ min and the yield of the reaction were determined.

## Supporting Information

Supporting Information is available from the Wiley Online Library or from the author.

## Acknowledgements

We acknowledge funding by Cariplo Foundation "ANTICARB - Quarry waste ANTIgorite CARBonation: a zero emission platform for re-manufacturing with the benefit of CO2 sequestration" (Grant no. 2020-0977); Italian Ministry of University and Research "Competing geological and biological processes in underground carbon and hydrogen storage" (Grant no. 20224YR3AZ); University of Milano - Bicocca "A nanotechnological approach for implementing circularity and carbon-neutrality in antigorite quarry industry" (Grant n. 2024-ATEQC-0017). Part of the work was performed with the support of Project MIUR - Dipartimenti di Eccellenza TECLA, Department of Earth and Environmental Sciences, University of Milano-Bicocca. We thank Paolo Gentile for his assistance during SEM analyses.

The Raman measurements have been performed at the Solid-Liquid Interface Nanomicroscopy and Spectroscopy laboratory (SoLINano-Σ LAB, https://www.polimi.it/en/research/laboratories/interdepartmental-laboratories/solinano-s-lab-solid-liquid-interface-nanomicroscopy-and-spectroscopy-lab) which is an interdepartmental facility at Politecnico di Milano.

We acknowledge Prof. Dr. Christian L. Lengauer (Universität Wien, Institut für Mineralogie und Kristallographie) for sharing with us crystallographic and Raman data relative to basic calcium carbonate. [Correction added on 15 May 2025, after first online publication: the order of references 20–45 has been corrected in this version.]

## Conflict of Interest

The autho declares no conflict of interest.

## Author Contributions

**Marcello Campione**: conceptualization (lead); funding acquisition (supporting); methodology (lead); supervision (lead); validation (equal); writing—original draft (equal); writing—review and editing (equal). **Daniela D'Alessio**: data curation (equal); formal analysis (equal); investigation (lead); software (equal); supervision (supporting); writing—review and editing (equal). **Mattia Corti**: investigation (equal); validation (equal); writing—review and editing (supporting). **Giancarlo Capitani**: data curation (supporting); investigation (supporting); methodology (supporting); validation (supporting); writing—review and editing (supporting). **Andrea Lucotti**: data curation (supporting); formal analysis (supporting); investigation (equal); validation (supporting); writing—review and editing (supporting). **Matteo Tommasini**: formal analysis (supporting); investigation (supporting); methodology (supporting); supervision (supporting); validation (supporting); writing—review and editing (supporting). **Rossella Yivlialin**: investigation (equal); software (equal); visualization (equal); writing—review and editing (supporting). **Lamberto Duò**: resources (supporting); supervision (supporting); writing—review and editing (supporting). **Gianlorenzo Bussetti**: funding acquisition (equal); project administration (equal); resources (supporting); supervision (supporting); writing—review and editing (supporting). **Nadia Malaspina**: funding acquisition (lead); project administration (equal); resources (equal); supervision (supporting); writing—review and editing (supporting).

## Data Availability Statement

The data that support the findings of this study are available from the corresponding author upon reasonable request.

## Keywords

brucite, carbon dioxide mineralization, carbonation catalysis, greenhouse gas emissions, hydrothermal conditions, microwave chemistry, portlandite

Received: February 3, 2025
Revised: April 21, 2025
Published online: May 11, 2025

[1] H. S. Santos, H. Ngguyen, F. Venâncio, D. Ramteke, R. Zevenhoven, P. Kinnunen, *Inorg. Chem. Front.* **2023**, *10*, 2507.
[2] R. Chang, S. Kim, S. Lee, S. Choi, M. Kim, Y. Park, *Front. Energy Res.* **2017**, *5*, 17.
[3] A. M. Chaka, A. R. Felmy, *J. Phys. Chem. A* **2014**, *118*, 7469.
[4] S. Atashin, R. A. Varin, J. Z. Wen, *J. Environ. Chem. Eng.* **2017**, *5*, 3362.
[5] F. P. Glasser, G. Jauffret, J. Morrison, J. L. Galvez-Martos, N. Patterson, M. S. E. Imbabi, *Front. Energy Res.* **2016**, *4*, 3.
[6] G. Montes-Hernandez, F. Renard, N. Geoffroy, L. Charlet, J. Pironon, *J. Cryst. Growth* **2007**, *308*, 228.
[7] G. Montes-Hernandez, A. Fernández-Martínez, L. Charlet, D. Tisserand, F. Renard, *J. Cryst. Growth* **2008**, *310*, 2946.
[8] H. Ho, A. Iizuka, *Adv. Energy Sustain. Res.* **2025**, 2400388.
[9] O. Qafoku, D. A. Dixon, K. M. Rosso, H. T. Schaef, M. E. Bowden, B. W. Arey, A. R. Felmy, *Environ. Sci. Technol.* **2015**, *49*, 10736.
[10] I. M. Power, P. A. Kenward, G. M. Dipple, M. Raudsepp, *Cryst. Growth Des.* **2017**, *17*, 5652.
[11] W. Dong, R. Liu, H. Zhao, X. Han, *Powder Technol.* **2020**, *360*, 741.

[12] G. Montes-Hernandez, M. Bah, F. Renard, *J. CO2 Util.* **2020**, *35*, 272.
[13] H. Nguyen, H. Santos, H. Sreenivasan, W. Kunther, V. Carvelli, M. Illikainen, P. Kinnunen, *Cem. Concr. Res.* **2022**, *153*, 106696.
[14] D. Toroz, F. Song, A. Uddin, G. A. Chass, D. Di Tommaso, *Cryst. Growth Des.* **2022**, *22*, 3080.
[15] D. Toroz, F. Song, G. A. Chass, D. Di Tommaso, *CrystEngComm* **2021**, *23*, 4896.
[16] X. Zhang, P. Alvarez-Lloret, G. Chass, D. Di Tommaso, *Eur. J. Mineral.* **2019**, *31*, 275.
[17] J. N. Boyn, E. A. Carter, *J. Am. Chem. Soc.* **2023**, *145*, 20462.
[18] M. Campione, M. Corti, D. D'Alessio, G. Capitani, A. Lucotti, R. Yivlialin, M. Tommasini, G. Bussetti, N. Malaspina, *J. CO2 Util.* **2024**, *80*, 102700.
[19] Z. Guo, W. Han, W. Zhao, L. Li, B. Wang, Y. Xiao, V. Alopaeus, *Powder Technol.* **2018**, *328*, 358.
[20] L. Bentea, M. A. Watzky, R. G. Finke, *J. Phys. Chem. C* **2017**, *121*, 5302.
[21] M. A. Watzky, R. G. Finke, *J. Am. Chem. Soc.* **1997**, *119*, 10382.
[22] F. Santoro De Vico, S. Bonilla-Correa, G. Pelayo-Punzano, K. Elert, C. Rodríguez-Navarro, E. Ruiz-Agudo, *Geochem. Perspect. Lett.* **2024**, *32*, 46.
[23] Q. Gautier, U. N. Berninger, J. Schott, G. Jordan, *Geochim. Cosmochim. Acta* **2015**, *155*, 68.
[24] D. L. Graf, *Am. Miner.* **1961**, *46*, 1283.
[25] G. Montanari, J. D. Rodriguez-Blanco, N. Bovet, S. L. S. Stipp, D. J. Tobler, *Cryst. Growth Des.* **2017**, *17*, 5269.
[26] X. Xu, Q. Lai, Y. Zhao, Y. Hao, H. Zeng, L. Wang, *Cryst. Res. Technol.* **2010**, *45*, 712.
[27] F. C. Meldrum, S. T. Hyde, *J. Cryst. Growth* **2001**, *231*, 544.
[28] M. Ripken, F. Gallien, T. Schlotterbach, C. L. Lengauer, *Eur. J. Miner.* **2018**, *30*, 85.
[29] H. W. Wang, L. L. Daemen, M. C. Cheshire, M. K. Kidder, A. G. Stack, L. F. Allard, J. Neuefeind, D. Olds, J. Liu, K. Page, *Chem. Commun.* **2017**, *53*, 2942.
[30] D. Gebauer, P. N. Gunawidjaja, J. Y. P. Ko, Z. Bacsik, B. Aziz, L. Liu, H. Yongfeng, L. Bergström, C.-W. Tai, T.-K. Sham, M. Edén, N. Hedin, *Angew. Chem., Int. Ed.* **2010**, *49*, 8889.
[31] K. J. Fricker, A. H. A. Park, *Ind. Eng. Chem. Res.* **2014**, *53*, 18170.
[32] K. A. Ofori, W. Hanson, K. Huang, L. Pan, *Miner. Eng.* **2024**, *219*, 109058.
[33] R. Rodríguez-Clemente, J. Gómez-Morales, *J. Cryst. Growth* **1996**, *169*, 339.
[34] P. J. Davies, B. Bubela, *Chem. Geol.* **1973**, *12*, 289.
[35] Q. R. S. Miller, H. T. Schaef, J. P. Kaszuba, L. Qiu, M. E. Bowden, B. P. McGrail, *Environ. Sci. Technol.* **2018**, *52*, 7138.
[36] M. Catti, G. Ferraris, S. Hull, A. Pavese, *Phys. Chem. Miner.* **1995**, *22*, 200.
[37] D. M. Henderson, H. S. Gutowsky, *Am. Miner.* **1962**, *47*, 1231.
[38] J. H. Park, S. H. Kim, J. C. Kim, B. Y. Choi, S. K. Kwak, O. H. Han, Y. Il Kim, S. W. Lee, *Chem. Eng. J.* **2021**, *420*, 130422.
[39] J. A. Koskamp, S. E. Ruiz-Hernandez, D. Di Tommaso, A. M. Elena, N. H. De Leeuw, M. Wolthers, *J. Phys. Chem. C* **2019**, *123*, 26895.
[40] J. L. Fulton, S. M. Heald, Y. S. Badyal, J. M. Simonson, *J. Phys. Chem. A* **2003**, *107*, 4688.
[41] P. D. Lundegard, Y. K. Kharaka, *Organic Acids in Geological Processes*, Springer, Berlin, Heidelberg **1994**, pp. 40–69.
[42] H. S. Santos, H. Nguyen, S. Illikainen, M. I. M. Alzeer, S. Cunha, P. Kinnunen, *Cryst. Growth Des.* **2024**, *24*, 7044.
[43] B. H. Toby, *J. Appl. Crystallogr.* **2001**, *34*, 210.
[44] *The Rietveld Method* (Ed: R. A. Young), Oxford University Press, Oxford **1993**.
[45] M. Akao, S. Iwai, *Acta Crystallogr. Sect. B* **1977**, *33*, 1273.